Available online at www.sciencedirect.com

ScienceDirect

IFAC PapersOnLine 58-13 (2024) 726–732

Stochastic Model Predictive Control for Robust Grid Frequency Regulation ⋆

Alexander Och * **Prof. Andreas Ulbig** *

* *IAEW at RWTH Aachen University, Aachen, Germany*
e-mail: {a.och; a.ulbig} @iaew.rwth-aachen.de

Abstract: This paper delves into the application of Stochastic Model Predictive Controls (SMPC) for power grids driven by inverter-interfaced generators, focusing on enhancing grid stability amidst decreasing inertia. By employing SMPC, uncertainties in energy systems are anticipated and plant-model mismatch is mitigated. Improvement in grid robustness concerning frequency limits is demonstrated via a Monte Carlo approach. The integration of data-driven model augmentation and stochastic constraint tightening significantly enhance the precision and robustness of frequency control. This study highlights the potential of SMPC in navigating uncertainties in energy systems and offering a robust framework for maintaining grid stability.

Keywords: Stochastic Model Predictive Control, Model Predictive Control, Frequency Regulation, Virtual Inertia, Droop Control, Data-Driven Modelling, Monte Carlo Approach

1. INTRODUCTION

In the wake of the global energy transition, the shift from conventional power generation to renewable energy sources is transforming the electrical grid at an unprecedented pace. This transformation, while crucial for sustainability, introduces significant challenges in maintaining grid stability due to the inherent decrease in system inertia as shown in (Ulbig et al. (2014)). The traditional grid, designed around synchronous generators, is facing adaptability issues e.g. frequency stability, necessitating the development of innovative control strategies for inverter-based resources. Grid-forming control strategies aim to emulate or enhance the inertia and damping properties traditionally provided by conventional generators.

This paper sets out to explore the development of new control algorithms for inverter-interfaced generators, focusing on their capability to supply synthetic inertia and support grid stability in low-inertia environments. Droop and VSM have been investigated extensively e.g. Muftau and Fazeli (2022) in this context. However, these approaches do not incorporate limitations like actuator saturation or operational limits. Furthermore, the DC-link is modelled as ideal voltage source with an infinite capacitance.

One solution is to expand the modelling in the classical VSM approach to matching the behaviour of an actual synchronous Machine Arghir et al. (2018). For this the equivalency between the physical energy storage of the rotating mass in a synchronous machine and the electrical energy storage in the capacitance on the DC-Link of the inverter is drawn. This model has been further developed to the Dual-Port Control to incorporate control loops for the DC-Link voltage and additional models of the of the DC-power source Subotić and Groß (2022) to exploit additional stabilizing feedback loops.

Virtual Oscillator Control (VOC) represents a transformative approach in the realm of grid-forming inverter control by simulating the dynamics of nonlinear oscillators, such as the Van der Pol oscillator. This method notably simplifies to a droop control mechanism in a quasi-steady state. The design of VOC however facilitates faster, more robust grid interactions and obviates the requirement for phase-locked loop mechanisms for frequency measurement Aghdam and Agamy (2022). Subsequent developments, such as the Dispatchable Virtual Oscillator Control Seo et al. (2019) aim to expand the VOC's functionalities to ensure flawless grid integration.

Another direction of research is utilizing an additional controller to adjust the conditional behaviour of the primary control consisting of the droop or the VSM. In (Markovic et al. (2019)) a dynamic adjustment of the inertia and damping terms of a VSM is proposed. Different operating regions are defined based on the Rate of Change of Frequency (RoCoF) and frequency deviations. Model Predictive Control (MPC) can be incorporated as an additional control layer to adjust power setpoints for the primary control. While decentralized controllers can enforce operational and actuator limitations central controllers can also coordinate participation among units (Stanojev et al. (2020)). A major challenge is to identify a prediction model for the frequency dynamics. While the latter uses a grey-box approach to estimate frequency dynamics in (Heins et al. (2022)) clear box model based on the frequency divider (Milano and Ortega (2016)) is proposed.

The potential of MPC as a control algorithm is widely recognised and extensive research has been conducted in the context of MPC for fast frequency regulation. However, rarely the issue of external disturbances and uncertainties caused by model-plant mismatch are addressed explicitly in MPC frameworks for frequency regulation. Typically, robustness for inverter-interfaced generation control is addressed through robust controller synthesis for uncon-

⋆ I would like to express my gratitude to Dr. Martina Josevski for her guidance and insightful feedback throughout my research.

10.1016/j.ifacol.2024.07.568

strained control (Bevrani et al. (2015)) or by focusing on the topic of energy management (Cominesi et al. (2017)). This gap has been partially addressed by recent work (Oshnoei et al. (2021)), and our study aims to further bridge this gap by enhancing an MPC for frequency regulation. For this purpose, the clear-box model MPC developed by Heins et al. (2022) should be extended with explicit stochastic models to account for uncertainties. The validity of theoretical guarantees should be investigated in the context of unknown uncertainty characteristics and sparse data. Their implications for a robust frequency regulation should be evaluated. The discoveries from the field of SMPC are reviewed and evaluated.

1.1 Literature Review

An intuitive way is to employ an estimator to determine the expected value of a disturbance as it is demonstrated in Anderson et al. (2019) where an unscented Kalman Filter is used to estimate interferences of remote grid-forming inverters on the decentralized control of the local grid-forming unit.

Another solution to mitigate this uncertainty is to use SMPC. SMPC is a method that directly incorporates uncertainties into probabilistic chance constraints and state predictions to manage uncertainties. Probabilistic chance constraints are in itself non-convex and must therefore be replaced to achieve a tractable optimization problem (Mesbah et al. (2019)).

The Polynomial Chaos Expansion (PCE) is able to handle parametric uncertainty and aims to improve prediction of the nominal state trajectory. The statistical moments of uncertain states are propagated using the moments of model parameters resulting in a prediction of the moments of future states which can also be used to tighten constraints (von Andrian and Braatz (2020)). This approach, however, assumes knowledge about the uncertainties' probability distributions (PD) which makes it largely impractical for frequency control applications.

Nonparametric approaches have been developed to enable generalized data-driven models. Uncertainties can be addressed explicitly by estimating an arbitrary nonconvex uncertainty set from data with nonparametric uncertainty estimation (Alexeenko and Bitar (2020)). Modelling the uncertainty with convex subsets then allows for a convex reformulation of chance constraints. The number of subsets can be chosen as a design variable and directly impacts the number of constraints.

The Data-Enabled Predictive Control (Coulson et al. (2019)) presents a fully nonparametric approach that eliminates the need for traditional system models. Instead, the optimization is performed with recorded past data and therefore addresses uncertainty implicitly. This approach has already been applied to inverter control by Huang et al. (2019). However, a significant challenge remains in the parametrization of the dataset used for optimization. The size of the dataset directly affects the number of constraints: small datasets may result in poor out-of-sample performance, while large datasets can greatly increase computational burden, making it impractical for time-critical applications.

Increased computational complexity can make Scenario-based approaches with explicit models (Schildbach et al. (2014)) impractical as well, even though the complexity can be addressed through set parametrization techniques (Rostampour and Keviczky (2018)).

The tightening constants can be estimated empirically based on samples. This however requires a sufficiently large number of samples to achieve a certain level of confidence (Bavdekar and Mesbah (2016)). To mitigate this problem Distributionally Robust Chance Constraints (DRCC) have been introduced. DRCC provide a certain level of constraint satisfaction for all PDs belonging to an ambiguity set. An interesting approach is presented in (Mark and Liu (2020)) where a limited number of data samples are used to create DRCC based on Wasserstein Ambiguity Sets.

The contribution of this paper is twofold. On the one hand it aims to investigate the accuracy of the approach proposed by Heins et al. (2022) by employing data-based estimations to improve the prediction model accuracy. The other goal is to investigate adaptive data-driven techniques to robustify the control against internal and external disturbances.

This paper is structured as follows: Section 2 explains the structure of the inverter control. Section 3 elaborates on the stochastic modelling approaches investigated. In Section 4 the findings of this investigation are presented and discussed. Section 5 concludes this paper and gives an outlook on possible future work.

2. INVERTER CONTROL STRUCTURE

In the course of this study, a hierarchical frequency control is investigated. A Model Predictive Control serves as a centralized coordinator for the distributed inverter-interfaced energy ressources. The decentralized control of the inverters provides virtual inertia via a droop control. The MPC adjusts the power setpoints for the inverter droop controlling their power infeed thus controlling their participation in the frequency regulation. This framework ensures coordination of power infeed for frequency regulation and enforces the frequency to stay within permitted bounds.

2.1 Decentralized Inverter Control

The control of the inverters in part utilizes the DC power flow approximations. But since the assumption of lossless lines does not necessarily hold for distribution grids a modification of active and reactive power.

$$P_{i,j} = U_i\, U_j\, \delta_{i,j}\, Y_{i,j} \tag{1}$$

$$Q_{i,j} = U_i\, (U_i - U_j)\, Y_{i,j} \tag{2}$$

Note that active and reactive power flows $P_{i,j}$ and $Q_{i,j}$ from bus i to bus j describe values modified according to De Brabandere et al. (2007). In the remainder of this paper, it will be referred to those modified values when addressing active and reactive power. The active power is proportional to the voltage phase angle difference $\delta_{i,j}$ between buses i and j respectively. The reactive power is proportional to the difference of voltage amplitudes U_i and U_j at buses i and j respectively. The line admittance between buses i and j is denoted with $Y_{i,j}$. Based on these proportionalities a frequency and voltage droop control is implemented as the outer control loops for the inverters.

$$\dot{\delta}_{\mathrm{drp},i} = \omega^* - m_{\mathrm{p}} \left(P_{\mathrm{gen},i} - P_i^* - \Delta p_i \right) \tag{3}$$
$$\dot{U}_{\mathrm{drp},i} = U_i^* - m_{\mathrm{q}} \left(Q_{\mathrm{gen},i} - Q_i^* \right) \tag{4}$$

The droop control calculates adjustments to frequency ω^* and voltage U_i^* setpoints based on the mismatch of their injected active $P_{\mathrm{gen},i}$ and reactive power $Q_{\mathrm{gen},i}$ and their corresponding external reference values $P_i^* + \Delta p_i$ and Q_i^* respectively. Those mismatches are scaled with the droop gains m_{p} and m_{q}. The resulting adjusted setpoints for frequency $\omega_{\mathrm{drp},i} = \dot{\delta}_{\mathrm{drp},i}$ and voltage U_{drp} are the reference values for the inner control loops. These inner control loops consist of cascaded voltage and current controllers which are realized with a PI-characteristic.

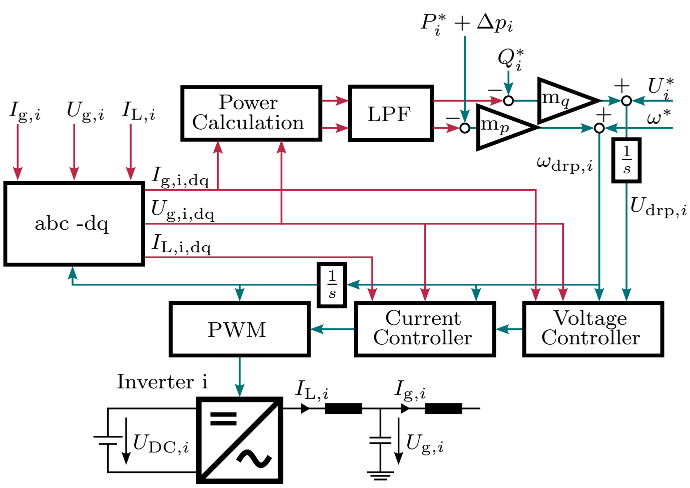

Fig. 1. Schematic of the Inverter Control

The structure of the decentralized inverter control is illustrated in Fig. 2 alongside the electrical model consisting of a DC-voltage source and LCL-output filter. The DC-voltage source is assumed to be constant and unaffected by the power injected into the grid. The reference for the active power consists of two parts. The nominal active power setpoint P_i^* is assumed to have an external source which is out of the scope of this paper. The power setpoint adjustment Δp is calculated by the centralized MPC coordinating the frequency regulation which is explained in the subsequent section.

2.2 Centralized Model Predictive Control

In order to retrieve an effective controller the design of the prediction model needs to be balanced between simplicity and accuracy. For this purpose, the dynamics of the inverter including inner control loops and filter are approximated with a PT1-element.

$$\tau_\omega \, \dot{\omega}_i = -\omega_i + \omega_{\mathrm{drp},i} \tag{5}$$

The interfacing frequency ω_i of inverter i can be described by the time constant τ_ω and the setpoint $\omega_{\mathrm{drp},i}$. In the course of this study the ω_i will be measured at the capacitor of the LCL-filter as the frequency of $U_{\mathrm{g},i}$. Equations 5 and 3 can be combined into 6. From equation 1 and the Frequency Divider formula from (Milano and Ortega (2016)) the dynamics of the injected power can be derived as equation 7.

$$\dot{\omega}_i = -\frac{1}{\tau_\omega}\,\omega_i - \frac{m_p}{\tau_\omega} P_i + \frac{m_p}{\tau_\omega} \Delta p_i + \frac{m_p}{\tau_\omega}\, P_i^* + \frac{1}{\tau_\omega}\,\omega^* \tag{6}$$
$$\dot{P}_i = \sum^{j \in N_i} U_i \, U_j \, Y_{i,j} \left(\omega_i - D_j \omega_G \right) \tag{7}$$

Where ω_G is the vector of all interfacing frequencies of the inverter buses and D_j is the row of the frequency divider matrix referring to Bus j. The indices of the buses connected to inverter i are contained in N_i. The voltage amplitudes at the connected buses are estimated with an extended Kalman Filter using measurements available at the inverter buses.

$$\min_{\Delta p, \epsilon_\omega, \epsilon_{\mathrm{r}}} \quad \|\Delta p\|_H^2 + G \left(\|\epsilon_\omega\|_\infty + \|\epsilon_{\mathrm{r}}\|_\infty \right) \tag{8a}$$
$$\text{s. t.} \quad x_{k+1} = A x_k + B \Delta p_k + \Gamma + E_k z_t \tag{8b}$$
$$\omega_{\min} - \epsilon_\omega + \gamma_k \le \omega_{k+1} \le \omega_{\max} + \epsilon_\omega - \gamma_k \tag{8c}$$
$$\Delta\omega_{\min} - \epsilon_{\mathrm{r}} \le \omega_{k+1} - \omega_k \le \Delta\omega_{\max} + \epsilon_{\mathrm{r}} \tag{8d}$$
$$P_{\min} - P^* \le \Delta p \le P_{\max} - P^* \tag{8e}$$
$$dP_{\min} \le \Delta p_k - \Delta p_{k-1} \le dP_{\max} \tag{8f}$$
$$\epsilon_r \ge 0, \quad \epsilon_\omega \ge 0 \tag{8g}$$

Equations 8a - 8g describe the full optimization problem for the MPC. The quadratic cost 8a comprises of the quadratic cost of controller action weighted with H as well as the slack costs with the penalty factor G for frequency and RoCoF constraints in 8c and 8d respectively. The prediction model consists of the discretized state space equations 6 and 7. The states are the frequencies and injected powers at the inverter buses. In addition, a correlative correction term E_k is introduced which is explained in Section 3.1. This correction also affects Γ. The frequency and RoCoF constraints 8c and 8d limit the frequencies and frequency changes in consecutive timesteps at the inverter buses respectively. Slack variables ϵ_ω and ϵ_r are introduced to guarantee feasibility. In addition, the constraint tightening terms γ_k are introduced which are explained in sections 3.2 and 3.3. The power setpoint constraint 8e ensures that the setpoint $\Delta p_i + P_i^*$ stay within the bounds of the feasible operating region of the inverter. Note that $P_{\min}$ and $P_{\max}$ are modified power values. Equation 8f limits the ramping rate of the inverter and the slack constraints 8g enforce positive slack variables. In the following section the methods to calculate the the model correction term E_k and the tightening terms γ_k based on stochastic modelling approaches.

3. STOCHASTIC MODELLING

This section introduces the stochastic modelling concepts that are being investigated in the scope of this paper. First, a Gaussian disturbance assumption is used to investigate potential for improvement by data-based modelling. Then the sample-based constraint tightening is explained which is used to robustify the MPC and subsequently the DRCC based on Wasserstein Ambiguity Sets are introduced.

3.1 Correlative Model Adjustment

To investigate correlations between information available at timestep t the vector of disturbances w_t is defined. w_t consists of the disturbances $w_{t+k|t}$ which are defined as the difference between the measured state x_{t+k+1} and the prediction using the measured state at timestep $t+k$ and the system model at timestep t.

$$w_{t+k|t} = x_{t+k+1} - A_t\, x_{t+k} - B_t u_{t+k} - \Gamma_t \tag{9}$$
$$w_t = [w_{t|t}^T, w_{t+1|t}^T, ..., w_{t+Hp-1|t}^T]^T \tag{10}$$

A joint Gaussian PD of w_t and the vector of available information $z_t = [x_t, w_{t-1|t-1}, z_t^*$ is assumed. $z_t^*]$ contains bus voltages and phase angles of inverter buses and their respective connected buses. The mean μ and covariance Σ of the Gaussian PD is estimated with a maximum likelihood approach and subsequently used to estimate the expected value of the disturbances $\hat{w}_t$ under the condition of z_t.

$$\mu = \begin{bmatrix} \mu_w \\ \mu_z \end{bmatrix} \tag{11}$$
$$\Sigma = \begin{bmatrix} \Sigma_{ww} & \Sigma_{wz} \\ \Sigma_{zw} & \Sigma_{zz} \end{bmatrix} \tag{12}$$
$$\hat{w}_t = \mu_w + \Sigma_{wz}\Sigma_{zz}^{-1}(z_t - \mu_z) = (\mu_w - E\mu_z) + E z_t \tag{13}$$
$$\tag{14}$$

The first part of equation 13 depends only on the arithmetic means μ_w and μ_z of w_t and z_t respectively and the correction matrix E. Those terms are constant and are incorporated in Γ in 8b. The correction matrix E contains the submatrices E_k corresponding to estimates of $w_{t+k|t}$ and is calculated with the covariance matrix for z_t and the cross-correlation matrix of z_t and w_t.

3.2 Sample-based Joint Chance Constraints

The tightening terms γ_k are calculated to robustify the frequency constraints 8c with joint chance constraints 15. The joint chance constraints enforce all frequencies at the inverter buses to stay within their bounds with a probability of at least $1-\epsilon$ given a the control input Δp. The probability level ϵ can be used as a design parameter to tune the robustness of the control.

$$\mathbb{P}[(\omega_{\min} \leq \omega_{k+t} \leq \omega_{\max})|\Delta p] \geq 1 - \epsilon \tag{15}$$

A convex reformulation of 15 can be derived analytically when the PD of the disturbance is known. Since the PD can not be derived a sample-based approach is applied. With samples of the error states $e_{t+k|t} = \omega_{t+k} - \omega_{t+k|t}$ the γ_k is tuned heuristically to fulfill equations 16 and 17 where I_g denotes the indicator function.

$$I_k^{(t)} = \begin{cases} 0, & \text{if } -\gamma_k \leq e_{t+k|t} \leq \gamma_k; \\ 1, & \text{otherwise.} \end{cases} \tag{16}$$

$$1 - \epsilon = \frac{1}{N_s} \sum_{t=1}^{N_s} I_k^{(t)} \tag{17}$$

The confidence of this estimation approach for γ_k grows with the sample size N_s as explained in (Bavdekar and Mesbah (2016)).

3.3 Distributionally Robust Chance Constraints

The chance constraints 15 can be generalized to consider more than one PD. These DRCC enforce probabilistic guarantees for all PD $\mathbb{P}$ belonging to an ambiguity set $\mathcal{P}$.

$$\inf\nolimits_{\mathbb{P}\in\mathcal{P}}\ \mathbb{P}[(\omega_{\min} \leq \omega_{k+t} \leq \omega_{\max})|\Delta p] \geq 1 - \epsilon \tag{18}$$

In (Mark and Liu (2020)) a data-driven approach is proposed based on the Wasserstein Ambiguity Set. According to their research a γ_k to fulfill 18 with a Wasserstein Ambiguity Set can be estimated with the linear program 19a-19d.

$$\min_{\alpha,\gamma}\ \frac{1}{N_s\epsilon}\sum_{t=1}^{N_s}\alpha_t + \gamma_{k,i} \tag{19a}$$
$$\text{s.t.}\ -\alpha_t - \gamma_{k,i} \leq -|e_{k+t|t,i}|, \quad \forall t \in \{1, ..., N_s\} \tag{19b}$$
$$-\alpha_t \leq 0, \quad \forall t \in \{1, ..., N_s\} \tag{19c}$$
$$\frac{1}{N_s}\sum_{t=1}^{N_s}\alpha_t \leq \epsilon - \beta\lambda \tag{19d}$$

The elements of γ_k can hereby be calculated for every constraint individually. α_t are auxiliary variables. The Wasserstein radius β and Wasserstein penalty λ are design variables. For their lower bound $\lambda\beta = 0$ the ambiguity set reduces to a single estimated PD i.e. 18 reduces to 15. For the upper bound of $\lambda\beta = \epsilon$ the tightening term $\gamma_{k,i}$ becomes $\parallel \mathrm{e}_{k+t|t,i} \parallel_\infty$.

4. RESULTS

The proposed control schemes have been tested and evaluated on an IEEE 9-bus system depicted in Fig. 2. The modelling was done with MATLAB/Simulink and an EMT simulation was used. To account for the stochasticity a Monte Carlo simulation is conducted where load steps of different magnitudes are performed to introduce external disturbances. The samples of the Monte Carlo simulations are then divided into n batches such that a set of $n-1$ batches is used as training data for the remaining batch in a cross-validation approach. Subsequently, the DRCC are calculated for every simulation separately without prior knowledge to investigate the approach's ability to handle sparse data.

4.1 Prediction Model

With the training data, the correlative model correction from Section 3.1 was calculated and then included in the state space equations for the prediction model. The state prediction was then compared to the state predictions in the base case i.e. $E_k = 0$. Mean μ_e and standard deviation σ_e of the frequency prediction errors for both cases are shown in Fig. 3 for every timestep in the prediction horizon.

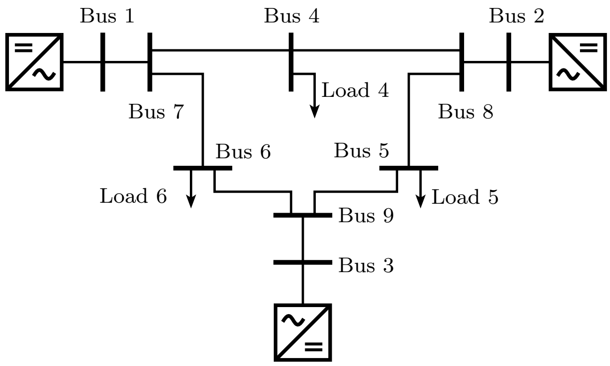

Fig. 2. The IEEE 9-Bus System

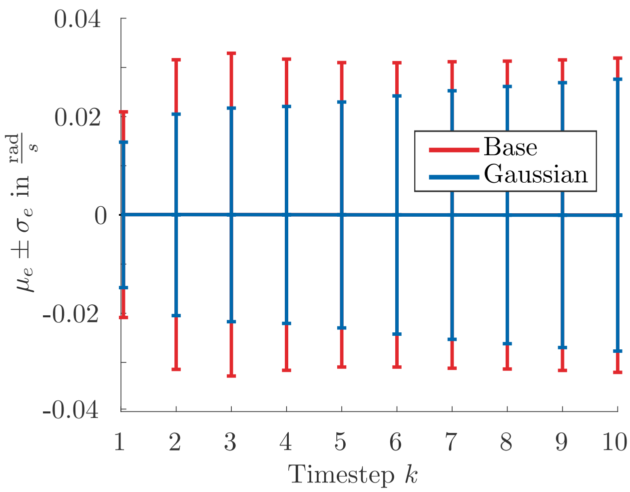

Fig. 3. Standard deviation for error frequency prediction

It can be observed that in both cases the prediction error is zero-mean but the correlative correction is able to decrease the prediction uncertainty. Which can be derived from the smaller σ_e. This improvement is largest for the first timesteps of the prediction horizon but remains significant throughout the prediction horizon. To investigate the impact of the improved prediction model the simulation is repeated with the adjusted controller. The effect on the individual constraints is illustrated in Fig. 4. The depicted histogram shows the difference in the number of total constraint violations across different violation magnitudes. Positive values indicate an increased number of constraint violations when applying the correlative correction term.

The histogram in Fig. 4 shows that the correction term actually increases the number of total constraint violations. Especially small violations occur significantly more often while the number of larger violations is reduced. Also, the histogram indicates an asymmetry in the disturbance estimation. This might result from the specific division into test and training batches and is up for investigation. For further comparison of the approaches, more metrics are presented in Table 1.

The results show that the improvement in prediction accuracy remains significant when the correction is part of the feedback loop. This leads to a decreased RMS value for the control input which is small but could be observed to be consistent across all batches. In addition, even though

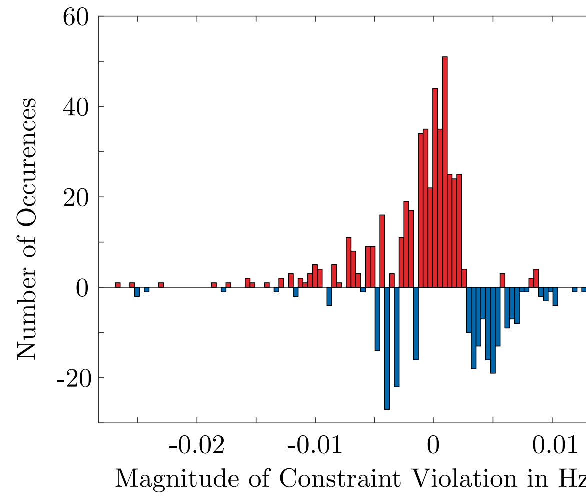

Fig. 4. Difference in the number of constraint violations

Table 1. Comparison of control with and without correlative correction

	Gaussian	Base
$\text{RMS}_{\Delta p}$	2783.3 VA	2807.8 VA
RMSE_{ω}	0.022536 $\frac{\text{rad}}{\text{s}}$	0.029477 $\frac{\text{rad}}{\text{s}}$
$\text{Vio}_{\%}$	11.06%	11.98%

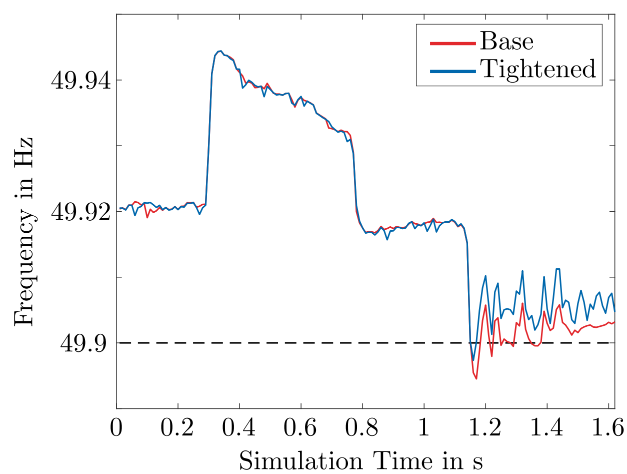

Fig. 5. Closed loop behaviour of the frequency

the total number of constraint violations is increased, the rate at which a frequency joint constraint violation occurs could be reduced by 9.23%. This can be explained with more simultaneous constraint violations.

4.2 Sample-Based Joint Chance Constraints

For the investigation of the constraint tightening the sample-based joint constraints were estimated from the training data for different probability levels ϵ. The simulations were then repeated with the tightened constraints. To illustrate the impact of the constraint tightening an exemplary closed-loop trajectory of a bus frequency is shown in Fig. 5.

Table 2. Impact of constraint tightening on the control objectives

ϵ	0	0.2	0.4	0.6	0.8
RMS_u[VA]	4142	3109	3010	2935	2877
$\mathrm{Vio}_{\%}$[%]	0.018	2.823	5.405	8.031	10.34

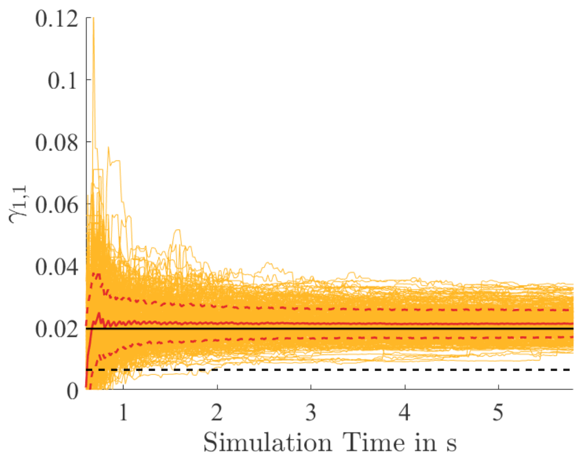

Fig. 6. Estimated tightening terms for sample-based joint chance constraints

The constraint tightening has a negligible effect on the trajectory as long as the frequency deviation is sufficiently small. As soon as the frequency approaches its minimum permitted frequency of 49.9Hz the constraint tightening enforces a tolerance band to prevent violations of the original constraint. The SMPC however allows constraint violations to a certain degree. The violation rate $\mathrm{Vio}_{\%}$ of the frequency constraints can be adjusted by tuning ϵ. The effect of ϵ on $\mathrm{Vio}_{\%}$ is presented in Table 2 alongside the RMS values of the control inputs.

The results show that the constraint violation rate reduces almost linearly with ϵ which suggests that the sample-based approach works as an unbiased estimator for γ_k. It also supports the assumption that nominal state and error state $e_{t+k|t}$ can be decoupled. The constraint tightening increases the robustness at the cost of a reduced solution space for the MPC which leads to larger input costs.

4.3 Adaptive Tightening

While the previous sections are based on prior collected samples this section relies only on samples generated during runtime. The propagation of an exemplary element $\gamma_{1,1}$ of the tightening term γ is presented in Fig. 6 for all simulations individually. The tightening term was calculated according to 4.2 with $\epsilon = 0.367$. In addition, the propagation of mean $\pm$ one standard deviation (dotted) of the estimated $\gamma_{1,1}$ are plotted in red. Two constant reference values are included as well. Both lines are calculated as sample-based chance constraints with all samples. The upper reference however refers to the joint chance constraints while the lower dotted line is calculated according to the individual constraints.

At the start of the simulation, $\gamma_{1,1}$ shows a high variance due to sparse data. However, after only two seconds the terms stabilize around the reference for the joint chance

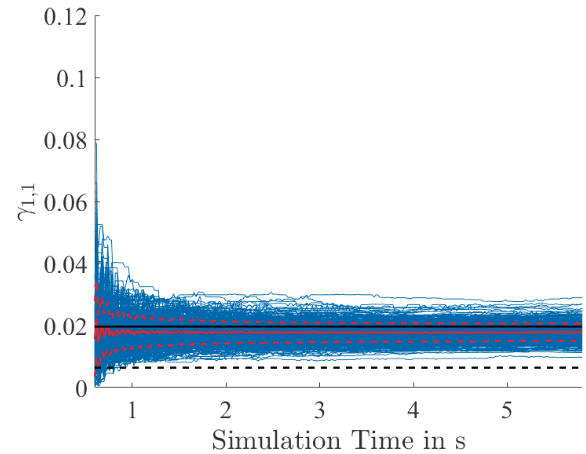

Fig. 7. Estimated tightening terms for distributionally robust chance constraints

constraints and proceed to converge towards this reference. The results of the comparative study based on DRCC with a Wasserstein penalty of $\lambda = 0$ is shown in Fig. 7.

It can be observed that even though the DRCC also introduce a moderate conservativism for $\lambda = 0$ the tightening tends to be less strict. This can be attributed to the fact that the DRCC refer to the individual constraints instead of the joint constraints. It should be noted however that the terms calculated according to the DRCC appear to be more compactly distributed compared to the basic sample-based approach. In theory, the conservativism can be tuned with Wasserstein penalty λ and distance β. In my investigation, I have observed no significant difference up to $\frac{\lambda\beta}{\epsilon} = 0.95$. From there the estimation became overly conservative with large variance and therefore meaningless.

4.4 Discussion

The significant improvement in the prediction accuracy indicates a succesful estimation of the disturbances. The external disturbances introduced by load steps are randomized and can be assumed to be uncorrelated to the operating point. Therefore this improvement should not be attributed to the prediction of external causes but rather indicate inaccuracies due to plant-model mismatch of the original controller. The sample-based constraint tightening has shown to be effective in robustifying the controller by a predefined rate when sufficiently large numbers of samples are available. For small sample sizes, the tightening lacks confidence. However, due to the high execution frequency of the MPC it can be assumed that a large number of samples can be retrieved within timeframes in which the grid can be assumed to have constant disturbance characteristics. Therefore, a sufficiently large number of samples to describe the disturbance characteristics can be assumed. Especially the handling of joint chance constraints makes this approach practical. The DRCC provide more conservativism and fast convergence properties. However, they are unable to handle joint chance constraints. This approach might be more suitable for a framework constraining only a single frequency like decentralized controllers or constraints on the Center of Inertia frequency.

5. CONCLUSION

This paper's exploration into SMPC for hierarchical frequency control of inverter-interfaced generators marks a significant advancement in addressing the challenges posed by the integration of renewable energy sources into the power grid. Through a comprehensive evaluation on an IEEE 9-bus system, it was demonstrated that the integration of data-driven model augmentation and stochastic constraint tightening significantly enhances the precision and robustness of frequency control. The results underscore the potential of SMPC in navigating the uncertainties inherent in energy systems, offering a robust framework for maintaining grid stability amidst decreasing inertia while providing guarantees on the constraint satisfaction on frequency limits. Reflecting on the journey from identifying the gap in current control strategies to developing and testing a novel SMPC approach, this study contributes a foundational step towards realizing more resilient power networks.

As we look to the future, further refinement of estimation techniques and exploration into decentralized approaches promise to unlock even greater potential in managing the complexities of tomorrow's energy landscape.

REFERENCES

Aghdam, S.A. and Agamy, M. (2022). Virtual oscillator-based methods for grid-forming inverter control: A review. *IET Renewable Power Generation*, 16(5), 835–855.

Alexeenko, P. and Bitar, E. (2020). Nonparametric estimation of uncertainty sets for robust optimization. In *2020 59th IEEE Conference on Decision and Control (CDC)*, 1196–1203. IEEE.

Anderson, S., Hidalgo-Gonzalez, P., Dobbe, R., and Tomlin, C.J. (2019). Distributed model predictive control for autonomous droop-controlled inverter-based microgrids. In *2019 IEEE 58th Conference on Decision and Control (CDC)*, 6242–6248. IEEE.

Arghir, C., Jouini, T., and Dörfler, F. (2018). Grid-forming control for power converters based on matching of synchronous machines. *Automatica*, 95, 273–282.

Bavdekar, V.A. and Mesbah, A. (2016). Stochastic nonlinear model predictive control with joint chance constraints. *IFAC-PapersOnLine*, 49(18), 270–275.

Bevrani, H., Feizi, M.R., and Ataee, S. (2015). Robust frequency control in an islanded microgrid: H_∞ and μ-synthesis approaches. *IEEE transactions on smart grid*, 7(2), 706–717.

Cominesi, S.R., Farina, M., Giulioni, L., Picasso, B., and Scattolini, R. (2017). A two-layer stochastic model predictive control scheme for microgrids. *IEEE Transactions on Control Systems Technology*, 26(1), 1–13.

Coulson, J., Lygeros, J., and Dörfler, F. (2019). Data-enabled predictive control: In the shallows of the deepc. In *2019 18th European Control Conference (ECC)*, 307–312. IEEE.

De Brabandere, K., Bolsens, B., Van den Keybus, J., Woyte, A., Driesen, J., and Belmans, R. (2007). A voltage and frequency droop control method for parallel inverters. *IEEE Transactions on power electronics*, 22(4), 1107–1115.

Heins, T., Joševski, M., Gurumurthy, S., and Monti, A. (2022). Centralized model predictive control for transient frequency control in islanded inverter-based microgrids. *IEEE Transactions on Power Systems*.

Huang, L., Coulson, J., Lygeros, J., and Dörfler, F. (2019). Data-enabled predictive control for grid-connected power converters. In *2019 IEEE 58th Conference on Decision and Control (CDC)*, 8130–8135. IEEE.

Mark, C. and Liu, S. (2020). Stochastic mpc with distributionally robust chance constraints. *IFAC-PapersOnLine*, 53(2), 7136–7141.

Markovic, U., Früh, N., Aristidou, P., and Hug, G. (2019). Interval-based adaptive inertia and damping control of a virtual synchronous machine. In *2019 IEEE Milan PowerTech*, 1–6. IEEE.

Mesbah, A., Kolmanovsky, I.V., and Di Cairano, S. (2019). Stochastic model predictive control. *Handbook of Model Predictive Control*, 75–97.

Milano, F. and Ortega, A. (2016). Frequency divider. *IEEE Transactions on Power Systems*, 32(2), 1493–1501.

Muftau, B. and Fazeli, M. (2022). The role of virtual synchronous machines in future power systems: A review and future trends. *Electric Power Systems Research*, 206, 107775.

Oshnoei, A., Kheradmandi, M., Muyeen, S., and Hatziargyriou, N.D. (2021). Disturbance observer and tube-based model predictive controlled electric vehicles for frequency regulation of an isolated power grid. *IEEE Transactions on Smart Grid*, 12(5), 4351–4362.

Rostampour, V. and Keviczky, T. (2018). Distributed stochastic model predictive control synthesis for large-scale uncertain linear systems. In *2018 Annual American Control Conference (ACC)*, 2071–2077. IEEE.

Schildbach, G., Fagiano, L., Frei, C., and Morari, M. (2014). The scenario approach for stochastic model predictive control with bounds on closed-loop constraint violations. *Automatica*, 50(12), 3009–3018.

Seo, G.S., Colombino, M., Subotic, I., Johnson, B., Groß, D., and Dörfler, F. (2019). Dispatchable virtual oscillator control for decentralized inverter-dominated power systems: Analysis and experiments. In *2019 IEEE Applied Power Electronics Conference and Exposition (APEC)*, 561–566. IEEE.

Stanojev, O., Markovic, U., Aristidou, P., Hug, G., Callaway, D., and Vrettos, E. (2020). Mpc-based fast frequency control of voltage source converters in low-inertia power systems. *IEEE Transactions on Power Systems*, 37(4), 3209–3220.

Subotić, I. and Groß, D. (2022). Power-balancing dual-port grid-forming power converter control for renewable integration and hybrid ac/dc power systems. *IEEE Transactions on Control of Network Systems*, 9(4), 1949–1961.

Ulbig, A., Borsche, T.S., and Andersson, G. (2014). Impact of low rotational inertia on power system stability and operation. *IFAC Proceedings Volumes*, 47(3), 7290–7297.

von Andrian, M. and Braatz, R.D. (2020). Stochastic dynamic optimization and model predictive control based on polynomial chaos theory and symbolic arithmetic. In *2020 American Control Conference (ACC)*, 3399–3404. IEEE.